Soft Matter

The buckling-condensation mechanism driving gas vesicle collapse

Journal:	*Soft Matter*
Manuscript ID	SM-ART-04-2022-000493.R1
Article Type:	Paper
Date Submitted by the Author:	22-Nov-2022
Complete List of Authors:	Zhao, Tom; Northwestern University Dunbar, Martha; Northwestern University Keten, Sinan; Northwestern University, Mechanical Engineering Patankar, Neelesh; Northwestern University, Department of Mechanical Engineering

Soft Matter

ARTICLE TYPE

Cite this: DOI: 00.0000/xxxxxxxxxx

The buckling-condensation mechanism driving gas vesicle collapse†

Tom Y. Zhao,[a,‡] Martha Dunbar,[a,‡] Sinan Keten,[a,b] and Neelesh A. Patankar [a,c]

Received Date
Accepted Date

DOI: 00.0000/xxxxxxxxxx

Gas vesicles (GVs) are proteinaceous cylindrical shells found within bacteria or archea growing in aqueous environments and are composed primarily of two proteins, gas vesicle protein A and C (GvpA and GvpC). GVs exhibit strong performance as next-generation ultrasound contrast agents due to their gas-filled interior, tunable collapse pressure, stability *in vivo* and functionalizable exterior. However, the exact mechanism leading to GV collapse remains inconclusive, which leads to difficulty in predicting collapse pressures for different species of GVs and in extending favorable nonlinear response regimes. Here, we propose a two stage mechanism leading to GV loss of echogenicity and rupture under hydrostatic pressure: elastic buckling of the cylindrical shell coupled with condensation driven weakening of the GV membrane. Our goal is to therefore test whether the final fracture of the GV membrane occurs by the interplay of both mechanisms or purely through buckling failure as previously believed. To do so, we (1) compare the theoretical condensation and buckling pressures with that for experimental GV collapse and (2) describe how condensation can lead to plastic buckling failure. GV shell properties that are necessary input to this theoretical description, such as the elastic moduli and wettability of GvpA, are determined using molecular dynamics simulations of a novel structural model of GvpA that better represents the hydrophobic core. For GVs that are not reinforced by GvpC, this analytical framework shows that the experimentally observed pressures resulting in loss of echogenicity coincide with both the elastic buckling and condensation pressure regimes. We also found that the stress strain curve for GvpA wetted on both the interior and exterior exhibits a loss of mechanical stability compared to GvpA only wetted on the exterior by the bulk solution. We identify a pressure vs. vesicle size regime where condensation can occur prior to buckling, which may preclude nonlinear shell buckling responses in contrast imaging.

1 Introduction

Gas vesicles (GVs) are gas-filled protein shells, found in aquatic bacteria or archea and used to regulate cell buoyancy[1]. The protein shell is cylindrical or lemon shaped, with biconical end caps enclosing the structure[2]. The cylindrical section is constructed primarily from a single 7.4 kDa amphiphilic protein, gas vesicle protein A (GvpA), wound in a continuous low-pitch helix approximately 4.6 nm wide and aligned to be nearly perpendicular to the longitudinal axis of the vesicle[2,3]. The interior of the GV appears to be hydrophobic, which prevents the liquid water from intruding into the cavity through pores in the membrane[1,4]. Hydrophilic gas vesicle protein C (GvpC) attaches to the outer surface of the GV and is expected to stabilize the vesicle wall[1,5,6].

Although GVs are intriguing protein assemblies in their own right, much of current research is motivated by their use as next generation biomedical tools. For instance, GVs have served as flexible non-invasive ultrasound contrast agents[7–11] and effective drug delivery vehicles[12,13]. Specifically, due to their stability, functionalizability, and gas filled interior, GVs can outperform traditional agents like microbubbles[7] as targeted nanoscale contrast agents for ultrasound[10]. Additionally, GVs have a tunable critical collapse pressure, p_e, at which the vesicle loses echogenicity and is presumed to either mechanically fail or fill with condensate. Both cases result in a decrease in turbidity. The pressure p_e associated with loss of echogenicity varies between bacteria and archea strains, and can be tuned in a variety of ways including removing or reintroducing GvpC[9,14,15], processing GVs with trypsin to cleave GvpC[14] and altering the surface charge[9]. Additionally, techniques to enhance ultrasound contrast by sequential collapse, or engineering non-linear and harmonic GV responses have been developed[7,8,16].

[a] *Northwestern University, Department of Mechanical Engineering: 2145 Sheridan Road, Evanston, Illinois 60208, USA*
[b] *s-keten@northwestern.edu*
[c] *n-patankar@northwestern.edu*

† Electronic Supplementary Information (ESI) available: ESI includes theoretical considerations for condensation, further discussion of GV width data available from experiments, and calculations related to condensation dynamics. See DOI: 10.1039/cXsm00000x/

‡ These authors contributed equally to this work

These techniques all rely on a predicable response to hydrostatic or ultrasonic input pressure, yet fundamental understanding of the collapse mechanism of the vesicle is limited. In literature, vesicle collapse has primarily been theorized to occur due to mechanical buckling of the protein shell under an applied hydrostatic pressure[1,8]. However, this mechanism does not consider the role of condensation within the vesicle and is subject to unconfirmed assumptions about the modulus and anisotropy of vesicle.

To elucidate the role of buckling in hydrostatic vesicle collapse, we use heterogenous nucleation theory (HNT)[17] to determine the critical pressure p_c above which condensation occurs within the vesicle (Figure 1a). In order to apply HNT, the surface wettability of the vesicle interior as measured by the intrinsic liquid-vapor contact angle θ_{int} must be known- this value determines the critical pressure p_c driving condensation. However, the interior contact angle of the GV membrane has not yet been quantified experimentally. Here, we apply molecular dynamics (MD) to simulate an all-atomistic GV wall from which θ_{int} can be pinpointed.

This leads to a deterministic relationship between the vesicle size, interior hydrophobicity, and the threshold pressure that drives condensation inside the vesicle. Aside from the loss of echogenicity when GVs are filled with water, we also show that wetting of the GV membrane on both the interior and exterior weakens its structural integrity by lowering the mechanical stability of the GvpA β sheets.

We also use analytical models of shell buckling to consider mechanical GV failure under hydrostatic pressure. The model we consider is pulled from the elastic stability analysis of cylindrical shells under hydrostatic pressure (both axial and circumferential) developed by Batdorf[18,19]. It has been previously noted that the β-strands of GvpA are tilted $\sim 54^\circ$ from the rib axis, resulting in the hydrogen bonds angled at $\sim 36^\circ$ from the rib axis. Ultimately, this leads to the transverse and longitudinal stress to be equivalent in the GV wall, and is known as the "magic angle"[1]. This feature would maximize the hydrostatic pressure a vesicle could be subjected to before mechanical failure *in vivo*, reaffirming that mechanical properties have been evolutionarily selected for; therefore, elastic buckling should be considered alongside HNT when studying GV failure. Additionally, we use a molecular model of the GV wall consisting of a planar assembly of GvpAs to investigate GvpA's response to mechanical deformation under different solvation states. Liquid water is known to decrease the mechanical response of β-strands[20], so insight into the effect of condensation on the GV mechanical integrity is necessary.

Overall, we aim to clarify the critical collapse mechanism from a unified perspective that considers multiple failure modes. We use molecular dynamics (MD) simulations to determine the liquid-vapor contact angle θ_{int} and the stiffness of the GV structure in the rib and axial direction. This MD input allows us to account for the effects of both buckling and condensation for GVs without GvpC. The analysis and modeling of GVs with GvpC binding across GvpA ribs is outside of the scope of this study. Focusing only on GvpA considerably simplifies the model and analysis, and many studies on echogenicity of GVs involved vesicles that consist only of GvpA.

We observe that as the applied exterior pressure p_{ext} increases for a vesicle of given dimensions, the elastic buckling pressure threshold p_b is reached first for larger vesicles with radii exceeding $R > 33.4$ nm. For GVs with radii smaller than this crossover value, the critical condensation pressure p_c is triggered first. This matches experimental data on the collapse pressure p_{exp} of GVs without GvpC, where $p_{\text{exp}} \approx \max(p_b,\ p_c)$. Thus, buckling and condensation appear to jointly determine the final fate of gas vesicles through rupture and/or loss of echogenicity.

We hypothesize that these dual mechanism may also explain the experimental observation that GVs stripped of GvpC exhibit preferred, nonlinear scattering in ultrasound that readily distinguishes from linear background signals. In the presence of GvpC stabilization, condensation may occur before elastic buckling due to GvpC reinforcement. Thus the loss of echogenicity precedes the onset of nonlinear buckling modes, and the weakening of the membrane walls under condensate contact can lead to rupture without a discrete pressure band associated with elastic buckling. When GvpC is removed, we show there exists a regime for larger vesicles where elastic buckling occurs before the critical condensation pressure p_c is reached. This elastic buckling mode can therefore generate nonlinear acoustic signals in the absence of interior condensate.

We also comment briefly on the connection between applied hydrostatic pressures and ultrasonic standing waves in driving vesicle response. The latter case is of more interest in recent applications using proteinaceous vesicles as acoustic contrast agents. Zhang et al.[21] showed that the resonance frequencies of both individual gas vesicles and GV agglomerates were significantly higher (in the order of GHz and 100s of MHz, respectively) than medically relevant ranges (10s or less of MHz). This suggests hydrostatic results may likewise inform buckling/condensation behavior under ultrasound conditions.

Extending nonlinear contrast in the elastic buckling regime before vesicle collapse occurs is highly desirable in GVs. Zhang et al.[21] definitively showed that buckling occurs prior to collapse, and also that the subharmonic and superharmonic pressure responses indicating nonlinear coupling occurred within approximately 20 kPa (or 6%) of the collapse pressure at 350 kPa for a specific vesicle species. In this regard, our analysis also reveals strategies for expanding this preferable nonlinear regime in view of the proposed rupture mechanism. The critical condensation pressure p_c can be delayed toward higher values to extend the elastic buckling regime; this may be accomplished by decreasing the wettability of the interior GV surface through functionalizing GvpA with additional hydrophobic residues or rendering the membrane impermeable to water molecules. Nonlinear signal enhancement may could also occur via deployment of larger GVs without GvpC as bioreporters. We observe that as the vesicle radius increases, the pressure bandwidth between p_b and p_c increases as well. This larger pressure range may enable elastic buckling without condensate formation.

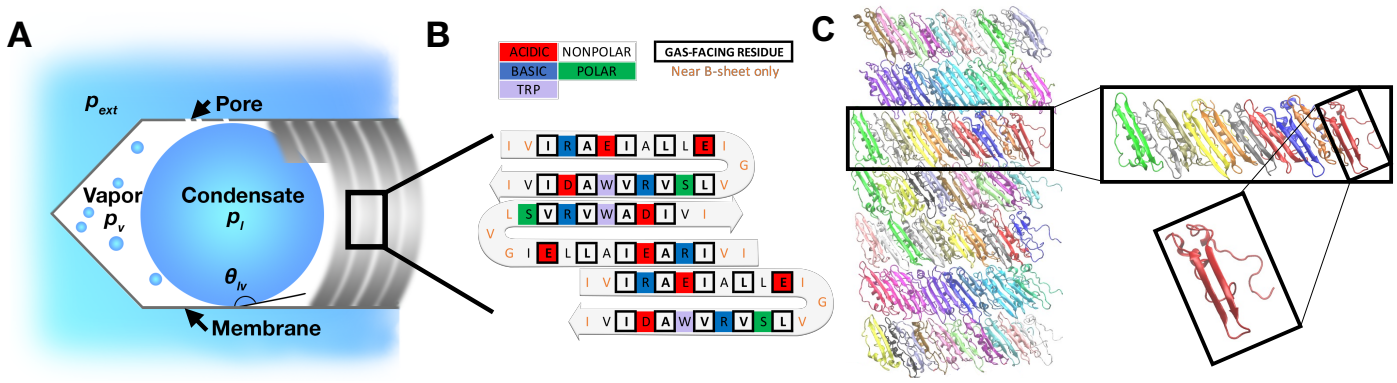

Fig. 1 A) Schematic cross section of vesicle structure. The system is assumed to be in thermodynamic equilibrium, the external liquid pressure, p_{ext}, is also equal to the liquid pressure of the condensate, p_l, since both are assumed to be in chemical equilibrium with the interior vapor. Pores in the membrane are permeable to water vapor. This permits the formation of liquid/vapor menisci with the same curvature as that of the condensate. B) GvpA β-sheet alignment along the rib ensures that the majority of residues facing towards the vesicle interior are hydrophobic to prevent nucleation. Salt bridges and $\pi-\pi$ interactions support the β-sheet structure. C) Visualization of top-down GV hierarchical structure, from entire wall to a GvpA rib to a single GvpA. Each GvpA protein is denoted in a different color.

2 Theory

2.1 Mechanism of Cylindrical Shell Buckling

The assumption in the literature is that mechanical buckling of the vesicle under hydrostatic pressure is the primary cause of vesicle rupture and the subsequent loss of echogenicity[1]. However, it has been shown that the critical pressure to induce elastic buckling can fall below the GV collapse pressure, especially when GvpC is stripped or cleaved from the vesicle[7]. Here, we identify an analytical model of the buckling in cylindrical shells in order to better understand this modality. Due to the high length-to-radius ratio of the GVs, a principal mode of collapse under external hydrostatic pressure is radial buckling of the cylindrical segment. Note that this leaves open the possibility that radial buckling of the conical end caps could be a source of overall collapse. This presumably occurs at a far higher pressure, but should be considered for completeness - the analysis is out of the scope of the current paper, but is ripe material for a future study. We can approximate the cylindrical portion of the vesicle as isotropic cylinders under external hydrostatic pressure, which become unstable due to elastic buckling at a critical pressure of[22]

$$p_b = \frac{0.855}{1-\nu^2}\left(\frac{E}{\left(\frac{R}{t}\right)^{5/2}\frac{L}{R}}\right), \tag{1}$$

where E is the isotropic Young's modulus, t is the ring thickness, R is the mean radius, L is the length of the cylinder, and ν is the poisson ratio. In this system, the hoop modulus can be approximated well by the tensile modulus of a single GvpA rib, since the membrane is very thin ($\sim$ 2 nm) and can be assumed to not support shear. Additionally, due to the low pitch helix of GvpA, we can approximate the material as isotropic. Since the Young's modulus of the shell protein GvpA has not been reported prior, we use steered molecular dynamics to estimate E (see Methods).

2.2 Mechanism of Condensation in Gas Vesicles

It has been experimentally demonstrated that small molecules, and specifically water, can diffuse freely into and out of the GV through pores in the membrane such that the vapor inside the vesicle is in equilibrium with the exterior cytoplasmic water[2]. Thermal equilibrium indicates that the temperatures of the exterior liquid and interior vapor are equal and constant at T. Similarly, chemical equilibrium implies the chemical potential of the vapor and liquid phases are the same, yielding[23]

$$p_V = p_{\text{sat}}\exp\left(\frac{V_L}{\Re T}(p_{\text{ext}}-p_{\text{sat}})\right), \tag{2}$$

where $\Re$ is the specific gas constant, V_L is the specific volume of the liquid, and the saturation pressure p_{sat} is only a function of the temperature T of the system. Given an externally applied pressure p_{ext} on the exterior liquid, the vapor pressure p_V inside the gas vesicle can be found from Eqn. 2.

After finding the equilibrium vapor pressure in the interior of the gas vesicle, we now examine the condensation mechanism. The energy barrier that must be overcome for condensation to occur inside the gas vesicle leads to a critical radius of the liquid nucleus[24]

$$r_c = \frac{2\sigma_{lv}}{p_{\text{ext}}-p_V}. \tag{3}$$

The expression for the critical radius r_c arises from the Young-Laplace equation describing mechanical equilibrium between the vapor phase and the liquid nucleus inside the vesicle across the curved two phase interface. Chemical equilibrium between the ambient vapor and the liquid nucleus inside the vesicle is given by

$$p_V = p_{\text{sat}}\exp\left(\frac{V_L}{\Re T}(p_L-p_{\text{sat}})\right), \tag{4}$$

where p_L is the equilibrium pressure of the liquid nucleus with radius r_c. Liquid droplets with radii smaller than the critical

value $r < r_c$ will disperse back into vapor, while droplets with radii greater than the critical size $r \geq r_c$ form nuclei that initiate growth of the condensed liquid phase.

To relate the critical nucleate radius for condensation r_c to the critical size of the gas vesicle R_c that permits the existence of such a nucleus, we recall that gas vesicles have cylindrical geometry with conical caps[1]. From heterogeneous nucleation theory, the relationship between the largest possible liquid droplet that can exist in mechanical equilibrium inside a cylindrical structure and the radius of the cylinder R_c is given by[24,25]

$$R_c = -r_c \cos(\theta_{\text{int}}) \tag{5}$$

where θ_{int} is the liquid-vapor contact angle. See the schematic in Figure 1a for reference. Thus, if the radius R of the gas vesicle satisfies $R < R_c$, the vapor phase is stable inside the vesicle and no phase change will occur. On the other hand if $R \geq R_c$, the vapor phase inside the vesicle will condense into liquid. Similarly, one can reverse this argument by starting from a given vesicle radius $R = R_c$ and arriving at the critical pressure that must be applied to the exterior liquid for condensation to occur inside the vesicle. This analysis is contingent upon knowing the contact angle θ_{int} of the gas vesicle, which has not been previously reported. To determine the liquid wettability of the inner hydrophobic vesicle walls, molecular dynamics is employed (see Methods). Prior literature on condensation within the vesicle is reviewed in Supplementary Information **??**.

3 Methods

3.1 GvpA Structure Generation

The GvpA structure has been previously predicted using *in silico* methods[26,27]; however, we elected not to use these structures due to the following reasons. The Ezzeldin et al. model predicted a GvpA structure with multiple charged residues facing the interior of the vesicle, which would result in a hydrophilic surface contrary to all experimental evidence. The Strunk et al. model appears to be much more accurate, however the GvpA rib structure that they obtained from Rosetta docking does not fully agree with NMR results which suggest that there are extensive inter-GvpA β-sheets[28]. Here, we utilized previously obtained NMR data[29] of an *Anabaena flos-aquae (Ana)* GvpA trimer to establish the structure of the β-sheet and turn regions. Next, we used Rosetta[30] and equilibrium MD simulations to produce a relaxed GvpA trimer. The Rosetta modeling score was found to be minimized with the 2 N- and C-terminus region α-helices centered on the hydrophilic face of the β-sheet.

From these GvpA trimers, a rib was constructed by replicating the relaxed trimer along the fiber axis. In this way, the segregation of hydrophobic and hydrophilic residues in the β-sheet region was maintained while aligning salt-bridges and π-π interactions between Trp residues. The rib was assembled in VMD[31] first in vacuum with neutralizing ions. Several ribs with increasing spacing between GvpA proteins were built and simulated to determine which was the most stable. Using the CHARMM36[32,33] force field in NAMD[34] the structure was minimized for 20000 steps and then equilibrated briefly with restrained backbone atoms for 20 ps. The protein structure was then moved to a liquid-membrane-vapor (LMV) or liquid-membrane-liquid (LML) interface with neutralizing ions, and neighboring ribs. In this notation, the first phase (eg. L for liquid) lies outside the vesicle, while the third phase (eg. V for vapor) is within the GV. TIP3P was used to solvate the systems[35]. Again, several offsets between ribs were simulated, and the spacing between ribs was decreased by 2 Å after each equilibration step until stable inter-rib interactions were formed. The fully periodic GvpA membrane was then equilibrated for 30 ns. After equilibration, another 10 ns production run was generated in order to gather information about the structures. Secondary structure content was calculated using the STRIDE algorithm[36].

3.2 Contact Angle Calculations

To find the liquid-vapor contact angle θ_{int} on the inner surface of the vesicle wall, molecular dynamics simulations were performed using LAMMPS[37]. First, a continuous film of water (5 nm thickness) was deposited on the flat hydrophobic side of the GvpA membrane built using the methodology described above. It is important to note that although the GvpA from *Anabaena flos-aquae* was used to build to GvpA membrane model, it has been shown that GvpA synthesized by different organisms are homologous, with similar amino acid sequences as well as secondary and tertiary structures[1]. Thus, it is expected that the material properties and contact angle would remain fairly uniform across different species. The system was then equilibrated at a constant temperature $T = 300$ K under a Nosé-Hoover thermostat. The explicit TIP3P water model was used for its ability to accurately capture the liquid/vapor surface energy[35]. Next, θ_{int} of the GvpA membrane interior was measured using a method presented in earlier work[25]. Briefly, the surface energies σ_{AB} between the various phase interfaces $A, B \in [L, V, M]$ of liquid, vapor and membrane were calculated using the stress tensor method[38] in molecular dynamics simulations with

$$\sigma_{AB} = L_z(P_N - \bar{P}_T), \tag{6}$$

where L_z is the length of the simulation domain normal to the interface, $P_N = P_{zz}$ is the normal component of the stress tensor with respect to the interface, and $\bar{P}_T = \frac{1}{2}(P_{xx} + P_{yy})$ is the average of the tangential components of the stress tensor. From eqn. 6, the ratio of surface energies can be used to find the intrinsic, equilibrium contact angle for liquid-vapor, membrane-liquid, and membrane-vapor (σ_{LV}, σ_{ML}, σ_{MV}) interactions via

$$\cos(\theta_{LV}) = \frac{\sigma_{MV} - \sigma_{ML}}{\sigma_{LV}}. \tag{7}$$

These calculations (eqn. 7) are repeated for both sides of the membrane, to examine the expected hydrophobic and hydrophilic contact angles for the interior and exterior faces of the vesicle, respectively. For visualization, a representative cross section of the GvpA membrane is shown in Figure 2.

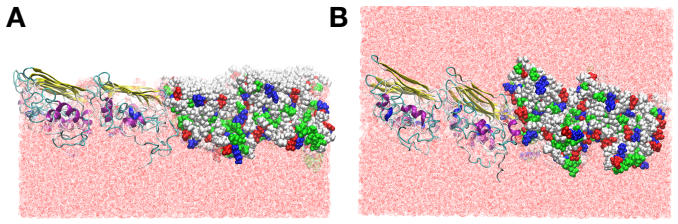

Fig. 2 A representative cross section of the A) LMV and B) LML systems. The cartoon representations are colored by secondary structure (where yellow, purple and teal represent β-sheet, α-helix and coil structure, respectively). The Van der Waals representations are colored by residue type (where white, blue, red and green represent hydrophobic, basic, acidic and polar residues, respectively). The full GvpA equilibrated sheet is composed of 9 ribs of 10 GvpA proteins each.

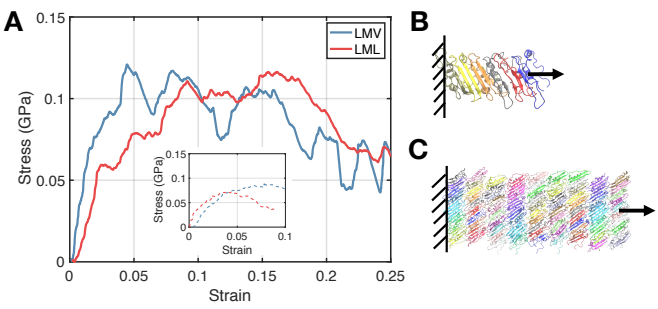

Fig. 3 A) The average intra-rib stress strain curve obtained over 5 independent trials for both the LMV and LML cases. The moduli were measured with a linear fit up to 0.02 strain, without specifying the intercept. The inset shows the inter-rib stress strain curve, from which the axial moduli were calculated. Next, a schematic of the B) intra-rib and C) inter-rib SMD simulations setup. The calculated moduli are found in Table 1.

3.3 Steered Molecular Dynamics

In an effort to quantify the mechanical properties of the GV wall, steered molecular dynamics (SMD) was performed on both GvpA rib and wall structures. For the rib simulations, short 6 GvpA rib segments were extracted from an equilibrated wall structure and re-equilibrated at a liquid-vapor or liquid-liquid interface with neutralizing ions. A soft harmonic restraint was applied to the α-carbons of the GvpA in order to prevent the structural rearrangement at the termini of the rib. After 2 ns of equilibration, the α-carbons in the β-sheet region of the first GvpA were fixed, and the α-carbons in the β-sheet region of the last GvpA were pulled. A similar approach was utilized to measure the modulus of the axial (inter-rib) direction. In this case a fully periodic membrane with 9 ribs was placed at a liquid-vapor or liquid-liquid and equilibrated for 10 ns. α-carbons in the β-sheet region of the first GvpA rib were fixed, and the α-carbons in the β-sheet region of the last GvpA rib were pulled. Steered molecular dynamics simulations were conducted with NAMD[34], at a velocity of 0.5 m/s. Earlier work suggests that this rate is small enough to obtain a converged estimate of the modulus[39]. Five independent trials were run for every case.

4 Results and Discussion

With an all-atomistic GvpA membrane model, it is possible to determine the liquid-vapor contact angle and the anisotropic mechanical properties. In order to calculate both the contact angle and the mechanical properties, a fully periodic GvpA membrane was built and then solvated in two ways to obtain a LMV and LML system (see Methods). The LMV case corresponds to the vapor phase occupying the vesicle interior. The LML case reflects liquid occupation of the GV, implying that condensation has occurred inside the vesicle.

By leveraging this model to determine the liquid-vapor contact angle, we can then use heterogeneous nucleation theory to determine the conditions required for condensation within the vesicle. Additionally, we can use SMD to predict the anisotropic material properties as input into an analytical shell buckling model. This allows us to determine the critical buckling pressure p_b associated with a gas vesicle. Note that recent study into the proper measurement of vesicle sizes has been incorporated into this study and reviewed in the Supplementary Information **??**.

4.1 Elastic Moduli

From SMD simulations, we can extract the axial and rib modulus by fitting a linear slope to the stress-strain curve up to 0.02 strain. These results are then incorporated into the analytical model for elastic buckling presented earlier. Overall, the LML and LMV cases do not have statistically significant differences in axial elastic moduli, giving ~2.5 GPa and ~2.6 GPa respectively. Note that this is, remarkably, reasonably similar to past predictions of the stiffness of phospholipid bubbles used in ultrasound contrast (3 GPa as found by Marmottant et al.[40]), used for similar applications.

However, note that the ultimate tensile stress and fracture strain for the LML gas vesicle system are significantly lower than that for the LMV system, suggesting that plastic failure would occur first for a vesicle wetted internally by condensate when all other parameters are equal.

Meanwhile, the intra-rib or hoop moduli appear to exhibit significantly larger differences between the LMV ($\sim$ 2.3 GPa) and and LML cases ($\sim$ 1.2 GPa). Thus the LMV system can withstand greater shell loading and would appear to delay rupture and plastic failure to higher hydrostatic pressures. Note also that Table 1 quantifies the error incurred by modeling the GvpA shell as an isotropic cylinder to be just over 10%. We take the effective elastic moduli of the system to be the larger axial quantity in order to give a conservative estimate of the system behavior.

These elastic moduli values are only slightly smaller than the reported mechanical properties of similar structural protein systems, such as amyloid fibers which are known for their mechanical performance ($\sim$ 9-27 GPa)[41]. The reduction in GV modulus could be accounted for by the lack of true cross-β structure as found in amyloids, where several β-sheets are oriented to form a solvent free cavity across which sidechain-sidechain interdigitation or interactions often occur. These interactions could provide additional stiffening that would not be available to the single β-sheet layer of GvpA.

Table 1 Mechanical Properties of GvpA Wall

Structure	Initial Length (nm)	Modulus (GPa) (± std. dev.)
Intra-Rib - LMV	5.83	2.3 ± 0.5
Intra-Rib - LML	5.49	1.2 ± 0.6
Axial - LMV	21.11	2.6 ± 0.2
Axial - LML	21.02	2.5 ± 0.3

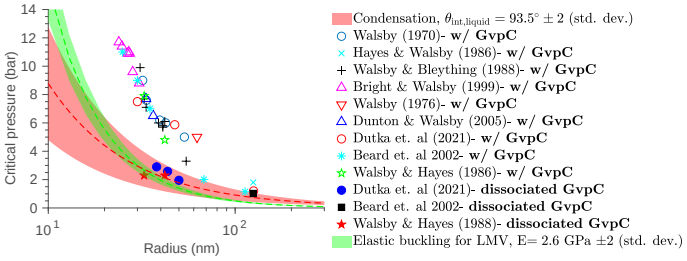

Fig. 4 The critical applied pressures associated with elastic buckling from instability theory[18,19], vesicle collapse from experiment[42–48], and condensation within the vesicle from HNT[25]. Experimental data are indicated by symbols corresponding to the paper the data point was retrieved from. Additionally, the buckling pressure relationship predicted using the elastic modulus extracted from SMD simulations are shown, where the range in green is a result of 2 standard deviations of the moduli for the LMV simulations. The range of the regions in red arise from the statistical uncertainty (2 standard deviations) in the value of the intrinsic contact angle $\theta_{int,liquid}$ estimated by molecular dynamics. It reflects θ_{int} of the hydrophobic interior, averaged for the cases where bulk liquid is in contact with the exterior, hydrophilic side of the membrane. No GvpC is modeled in this calculation. Other water properties at $T = 300$ K were obtained from NIST[49], including the surface tension $\sigma_{lv} = 0.07169$ N/m, the specific gas constant $R = 461.5$ J/(kg K), specific volume $V_L = 0.001004$ m^3/kg and the saturation pressure $p_{sat} = 0.035368$ bar. For the buckling analysis, we took the length of the GV membrane to be 500 nm and thickness as 2.5 nm. The thickness of the GV is commonly reported to by 1.8 nm[1], however, we found that the equilibrated model had a thickness closer to 2.5 nm.

4.2 Relationship between Critical Collapse Pressure and Vesicle Size

To determine the wettability of the membrane, we calculated the contact angle of both the interior and exterior of the GvpA protein shell using equilibrium MD simulations.

The interior contact angle of the membrane is $\theta_{int,liquid} = 93.5° \pm 0.8°$ when the exterior is solvated by bulk liquid water; this represents vesicles immersed in aqueous solution. When the exterior phase is vapor, reflecting vesicles present in a non-aqueous setting, the interior contact angle reaches a higher value $\theta_{int,vapor} = 99.0° \pm 0.9°$.

We note two salient points. First, the interior surface of the vesicle is hydrophobic, as expected from both its residue makeup and experimental observations[1]. Secondly, the difference between $\theta_{int,vapor}$ and $\theta_{int,liquid}$ suggests that the environment on the opposite side of the membrane has a significant effect on the interior wall wettability. This dependence is subsequently examined to estimate the effective contact angle of the inner membrane surface when GvpC binds to the exterior.

For completeness, the exterior contact angle of the membrane was found to be $\theta_{ext,vapor} = 87.7° \pm 0.9°$ when the interior is filled with vapor, and $\theta_{ext,liquid} = 70.3° \pm 1.7°$ when the interior is filled with liquid. These MD calculated values match experimental observations[1] that the exterior surface is hydrophilic.

4.3 Pressure Radius Relationship

Using this structural information from MD, the critical hydrostatic pressure p_c driving condensation within the vesicle (eqn. 5), the threshold pressure p_b for elastic buckling (eqn. 1), and the experimental collapse pressures p_{exp} are visualized in Figure 4 as a function of the vesicle radius. For GVs with GvpC dissociated from the GvpA shell, the critical pressures for elastic buckling and condensation appear to be in close proximity.

The two critical curves $p_b(R)$ and $p_c(R)$ intersect at a vesicle diameter of 33.4 nm and a pressure of 2.6 bar. Below this crossover radius (or above the crossover pressure), condensation occurs before elastic buckling as the applied pressure is ramped up. We hypothesize that these GVs will not experience a band of pressures where elastic buckling can generate nonlinear signals, as the liquid water on both sides of the membrane would damp out such oscillations or the vesicle would rupture upon hitting the buckling threshold p_b due to wall weakening. Above this crossover radius, there exists a pressure band in which elastic buckling occurs before condensation as the applied pressure increases. We hypothesize that this regime permits the nonlinear, elastic buckling seen in experiment[16]. Indeed, Zhang et al.[21] showed via laser Doppler vibrometry that vesicles with radii above 100 nm demonstrate reversible buckling behavior before final collapse.

Thus we propose a coupled, two stage mechanism for ultimate GV rupture. Interior condensation facilitates wall weakening due to wetting of the inner GvpA shell. The liquid occupation of the vesicle reduces the ultimate tensile strength and fracture strain in the axial direction as well as decreases the elastic modulus and yield strength in the circumferential direction. It also causes a loss of echogenicity independent of GV collapse.

Elastic buckling of the weakened wall likely induces final vesicle rupture. This conclusion agrees with ultrasound data[16], which shows that sinusoidal acoustic pressure applied at wavelengths lower than the filling time of the vesicle (around 2 ms, as derived in Supplementary Information **??**) requires significantly larger peak amplitude than the hydrostatic pressure p_{exp} to cause GV collapse. However, acoustic pressures exceeding the hydrostatic p_{exp} are sufficient to trigger reversible elastic buckling that results in a nonlinear response. This suggests condensation plays an important role in bridging elastic buckling with final vesicle failure.

4.4 Response to ultrasound

Since gas vesicles are featured in recent application as acoustic contrast agents, their collapse behavior under oscillatory pressurization by ultrasound is of particular interest. Here we model the acoustic signal as a standing plane wave with amplitude A, angular frequency ω, and wavelength λ. The ultrasonic standing wave exerts an acoustic radiation force in the axial normal direction to particles suspended in an aqueous solution, and an

acoustic streaming force in the tangential shear direction[50].

As calculated by Yosiok et al.,[51] the maximum amplitude of the acoustic radiation force exerted upon a vapor bubble of radius R_{bubble} held at isothermal conditions is:

$$F_{\text{radiation}} = \frac{\pi A^2 \lambda R_{\text{bubble}}^3}{\rho c^2} \left(\frac{(1/c_f^2)(3\rho_f - (\lambda R_{\text{bubble}}/c_f)^2)}{c_f^2(\lambda R_{\text{bubble}}/c_f)^6 + (3\rho_f - (\lambda R_{\text{bubble}}/c_f)^2)^2} \right), \quad (8)$$

where c_f & ρ_f are the ratio of sound speed & density in the vapor bubble to the corresponding values in the ambient liquid, and ρ & c are the density & sound speed of the surrounding liquid medium.

Although the gas vesicle membrane exhibits different modes of oscillation than a bubble under an impinging ultrasonic wave, the response of a cylindrical shell is not tractable to a closed form solution and requires numerical simulation to resolve[52]. Here, we approximate the behavior of a gas vesicle to that of bubble as an order of magnitude estimate of the acoustic radiation pressures involved.

From Shapiro group,[43] we reference representative values of the radius $R \in [160, 204]$ nm, hydrostatic collapse pressure $p_{\text{exp}} \approx$ 64 kPa, and ultrasonic collapse pressure $p_{\text{ult}} \approx 576$ kPa applied at a frequency f of 12.5 MHz[8] for Halobacterium salinarum gas vesicles. The acoustic radiation pressure $P_{\text{radiation}}$ is determined by normalizing the force in eqn. 8 by the projected area $2RL$, where $L = 400$ nm[8] is the length of the cylindrical vesicle shell. Using values for a liquid water medium at 300 Kelvin, we find $P_{\text{radiation}} \approx 22$ kPa, which is in the same order of magnitude as the hydrostatic collapse pressure 64 kPa. This suggests that similar buckling/condensation mechanics drive vesicle collapse under both ultrasonic and hydrostatic scenarios.

On the other hand, the shear oriented acoustic streaming stress exerted upon a bubble was modeled by Rooney[53] as

$$\tau_{\text{streaming}} = 2\pi^{3/2} \left(\frac{A}{\rho c} \right) \left(\frac{\rho \mu}{f} \right)^{1/2} \frac{1}{R_{\text{bubble}}}, \quad (9)$$

where μ is the viscosity in the liquid medium. For an aqueous environment at 300 Kelvin, we find $\tau_{\text{streaming}} \approx 2$ kPa, which is one order of magnitude smaller than the normal acoustic radiation pressure.

Thus the tangential shear stress within the boundary layer adjacent to the vesicle membrane is negligible compared to the axial radiation pressure. In the context of ultrasound application, we thus expect pressure driven buckling/condensation to dominate vesicle collapse dynamics, rather than any shear driven instabilities.

4.4.1 Acoustic resonance

Sharma et al.[54] studied the free vibration of cylindrical shells at their resonance frequencies. In particular, the uniform rubber shells they considered appear to have longitudinal elastic moduli at the same order of magnitude as the GvpA proteins considered in this work. The acoustic response at the resonance frequencies of these cylindrical shells were not significantly different (within the same order of magitude) compared to excitation away from these monopole modes.

We attibute this behavior to the nonhomogeneous moduli exhibited by the gas vesicle protein in tension (which we measured) compared to in compression (typically less stiff for most proteins); additionally, the non-axial protein orientation along the vesicle wall means that the effective longitudinal vs radial moduli would be sufficiently different, such that no single monopole mode dives unbounded resonance response.

This qualitative description is borne out by the experimental data from Zhang et al.[21]. They show that the actual resonance frequencies of individual vesicles (on the order of GHz) and GV agglomerates (on the order of 100 MHz) are significantly higher than medically relevant ultrasound frequencies (10s or less of MHz). This suggests that conclusions draw from hydrostatic analysis may be applicable to practical ultrasonic scenarios. Moreover, the maximum wall displacement driven by these resonance modes are typically less than 1% of the vesicle radius, which agrees qualitatively with the muted response of cylindrical shells to resonance forcing described previously.

4.5 Influence of GvpC

GvpC makes up around 9% of the GV by mass and influences vesicle behavior in important ways. The assumption in literature is that GvpC strengthens the GvpA membrane, perhaps by acting like a mechanical spring or stiffener[2,44]. It is known that when GvpC is present, the critical collapse pressure is higher than when it is absent (Figure 4)[6]. Lakshmanan et al. observed that when GvpC is stripped from the exterior of the GV the collapse pressure of the vesicle decreases[9], but it can be reintroduced with very little change to the critical collapse pressure[15].

It is also known from trypsin digest experiments that GvpC is found on the exterior of the membrane[14], but the way that GvpC is attached to the GvpA membrane is entirely unknown, with some speculation that it is wrapped in the opposite direction to the GvpA rib[55]. Additionally, GVs produced from genes with the portion that encode GvpC removed have odd shapes, and increase/decrease in diameter non-uniformly[56]. Finally, while the exact GvpC structure is not known, it is known to have extensive α-helix regions[55].

Although a reasonable GvpC structure can be predicted from homology modeling, accurately docking it on the surface of GvpA is an intractable problem due to the size of the system and the absence of experimental insight. Thus, the modeling of the GvpC protein is out of the scope of the present work.

In order for the critical collapse pressure to vary reversibly when the presence or absence of GvpC, this protein must have change the properties of the wall. Here, we propose two possible avenues for how bound GvpC affects the structural stability of the GV.

Note that the purpose of this section is to speculate about the role of GvpC in modulating the buckling and condensation response to applied hydrostatic pressure, without actually simulating GvpC (due to the lack of available NMR data in the literature

as well as the limited computational scope of the current work).

4.5.0.1 Condensation For condensation, GvpC appears to have two major effects on the wettability of the membrane interior. We have already noted a significant change in the inner shell surface contact angle depending on the exterior environment. The binding of GvpC to the GvpA membrane is expected to buffer the interior wettability to some extent, such that $\theta_{\text{int,liquid}} \leq \theta_{\text{int,GvpC,liquid}} \leq \theta_{\text{int,air}}$ To estimate the effect of this second protein layer, we bound GvpA protein to the exterior of the original GvpA shell and found the interior contact angle to be $\theta_{\text{int,GvpA,liquid}} = 97.8^\circ \pm 1.1^\circ$ when the exterior phase was liquid water. The critical condensation pressure $p_{e,\text{GvpA}}$ corresponding to this configuration is visualized in Fig. 5; it seems to capture the experimental collapse pressure for GVs with bound, intact GvpC. From this first mechanism, we hypothesize that $\theta_{\text{int,GvpC,liquid}} \lesssim \theta_{\text{int,GvpA,liquid}}$ and would yield a corresponding condensation pressure $p_{e,\text{GvpC}} \lesssim p_{e,\text{GvpA}}$.

Secondly, the presence of GvpC may also cause a localized torsion angle change of the glutamic acid residue near the β turn, inducing it to face the exterior side of the membrane. Namely, the glutamic acid near the β turn is the only charged amino acid predicted to face the interior of the vesicle (see Figure 1B) and our MD simulations demonstrated that its removal increased the contact angle. This mechanism could also increase the hydrophobicity of the interior wall when GvpC binds to the GV.

4.5.0.2 Elastic Buckling Mechanical stiffening is the other possible reason critical collapse pressure increases when GvpC is present. In this case, it is hypothesized that the α-helix of GvpC could act as a spring to resist deformation. It is not unreasonable to expect a majority α-helix structure like GvpC to have an elastic moduli on the order of gigapascals[39]. If GvpC binding homogeneously strengthens the cylindrical shell, it would need to boost the effective elastic modulus to around 6 GPa for the threshold elastic buckling pressure to reach the same order of magnitude as experimental collapse pressures of GVs with bonded GvpC.

If GvpC binding can be modeled as local ring stiffeners strengthening the underlying GvpA membrane, a back of the envelope calculation using the mass percentage of GvpC (9%[42]) can estimate the associated threshold elastic buckling pressure. Assuming the density of GvpC ρ_C is about the same as that of GvpA ρ_A, the volume V_c of the GvpC protein in a vesicle can be found by

$$V_c = (0.09)\rho_C \left(\pi(R+t)^2 L - \pi R^2 L\right). \tag{10}$$

If the thickness of this GvpC stiffener is comparable to that of the GvpA shell t, the combined length h of all GvpC bound to the exterior is

$$h = \frac{V_c}{\pi(R+2t)^2 - \pi(R+t)^2}. \tag{11}$$

Finally, we can express the distance d between two ring stiffeners as

$$d = \frac{L-h}{a-1}, \tag{12}$$

where a is the total number of GvpC stiffeners distributed on a single GV. The cross-sectional area A_s of each stiffener is therefore

$$A_s = td \tag{13}$$

The threshold pressure p_s for elastic buckling of an isotropic cylinder strengthened by stiffeners is given via[19]

$$p_s = \frac{5.513}{LR^{3/2}} \left(\frac{1}{\frac{Et}{1-\nu^2} + \frac{E_r A_r}{d}}\right)^{\frac{1}{4}} \left(\left(\frac{Et^3}{12(1-\nu^2)} + \frac{E_r I_r}{d} + \tilde{z}_r^2 \frac{E_r A_r}{d}\right)^3 \left(\left(\frac{Et}{1-\nu^2} + \frac{E_r A_r}{d}\right)\left(\frac{Et}{1-\nu^2}\right) - \left(\frac{\nu Et}{1-\nu^2}\right)^2\right)\right)^{\frac{1}{4}}, \tag{14}$$

where I_r is the moment of inertia of the stiffener around its centroid and $\tilde{z}_r$ is the stiffener eccentricity. Note that the number of stiffeners a is undetermined. Here, we take the elastic buckling pressure of ring stiffened GVs $p_{b,\text{ring}}$ to be the maximum p_s with respect to all possible integer choices of a. This yields a distance $d \approx 29$ nm between GvpC stiffeners.

With these assumptions, the elastic buckling pressure $p_{b,\text{ring}}$ of a ring stiffened GV is significantly larger than p_b of the simple unstiffened isotropic cylinder model, even when the elastic modulus of GvpC is estimated to be the same as that of GvpA. Fig. 5 shows that $p_{b,\text{ring}}$ provides a better estimate of the experimental collapse pressures for GVs with bound GvpC. Thus the presence of GvpC can alter the structural stability of the vesicle by providing both mechanical stiffening as well as condensation delay through increased hydrophobicity of the inner GvpA wall. If the presence of GvpC did not affect interior wettability, we would expect to observe loss of echogenicity at much lower pressures than those observed experimentally; essentially, the presence of GvpC would not affect the collapse pressure since condensation would occur regardless of how effectively GvpC can serve as stiffeners.

For GvpC bound vesicles, we also observe a crossover between the buckling driven failure regime and condensation driven failure regime at the vesicle radius $R \approx 541$ nm and applied pressure 0.3949 bar. That is, below this critical size (or above this crossover pressure), condensation could occur first within the vesicle as the external pressure ramps up, thereby compromising the shell membrane. Thus there exists no band of pressures corresponding to reversible buckling for vesicles smaller than this crossover radius; upon reaching the critical buckling pressure, the vesicle immediately collapses due to pre-weakening of the walls by interior condensate, which is supported by experimental data in Fig. 5.

Fig. 5 also shows that above the crossover radius for GvpC bound vesicles, buckling can occur before condensation. We therefore observe experimental collapse pressures that significantly exceed the critical buckling pressure, which permits the existence of a favorable, reversible buckling regime. Then as internal condensate weakens the vesicle membrane upon applying larger external pressure that exceeds the critical condensation threshold, the vesicles of size greater than the crossover radius collapse.

This clear description of the interacting mechanisms of conden-

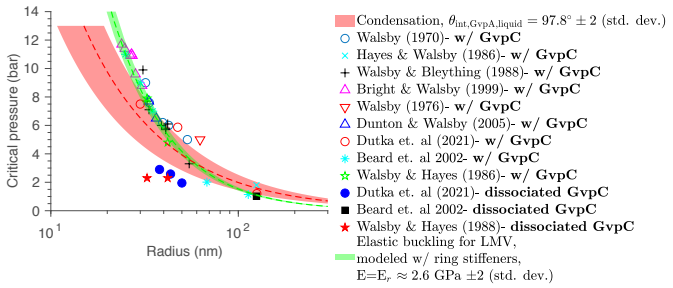

Fig. 5 The vesicle collapse pressure from experiment p_{exp} [42–48], the critical condensation pressure $p_{c,GvpA}$ of the GV with a second layer of GvpA [25], and the critical buckling pressure $p_{b,ring}$ for ring stiffened GVs, as a function of the GV radius. Experimental data are indicated by symbols corresponding to the paper the data point was retrieved from. The range of the regions in red arise from the statistical uncertainty (2 standard deviations) in the value of the intrinsic contact angle $\theta_{int,GvpA,liquid}$ estimated by molecular dynamics. It represents the contact angle of the hydrophobic interior, averaged over the cases where bulk liquid is in contact with the exterior, hydrophilic side of the membrane. A second layer of GvpA is bound to the outside of the first GvpA layer to explore the effect of protein buffering on interior wettability. The buckling pressure of a ring stiffened cylindrical shell is used to model the presence of GvpC bound to the outer GvpA shell. The elastic modulus, density, and thickness of the GvpC stiffeners are assumed to be the same as those of GvpA.

sation and buckling also may explain why we observe better reversible buckling performance for vesicles stripped of GvpC. The crossover radius for vesicles without GvpC (33.4 nm) is an order of magnitude smaller than that for vesicles with bound GvpC (514 nm), while the crossover pressure is one order of magnitude larger. This means a broader size range of vesicles can access the preferred reversible buckling paradigm under less stringent applied pressure conditions for vesicles with stripped GvpC.

This breakdown of collapse mechanics also enables more informed vesicle design to select for favorable behavior in drug delivery and bioreporting application. The analytical specification of the crossover radius for wild-type and engineered vesicles as a function of their membrane wettability, moduli, and exterior functionalization permits, for instance, flooding of gas vesicles prior to collapse, such that a small molecule drug load is thoroughly pre-dissolved and may not adhere to the vesicle wall upon buckling collapse. Alternatively, the reversible buckling regime can be extended to enhance medical imaging resolution by extending the pressure band between pre-buckling and post-condensation after the analytically determined crossover- or choosing different vesicle species that occupy different reversible-buckling bands to enable multi organ targeting.

Before concluding this section, we note that assuming GvpC act as local ring stiffeners to stabilize the vesicle membrane is purely speculation. The authors are not aware of a definitive answer as to how GvpC actually stiffens the gas vesicle. In most recent applications as ultrasound contrast agents, the typical modus operandi is to simply strip GvpC from the vesicle to access preferred nonlinear harmonic modes. We can similarly strip the discussion of GvpC from the current paper to avoid speculation that can be later proven false by new studies, but that seems rather defeatist and does not stimulate interest or further investigation into the role of GvpC.

Walsby in his seminal review [57] speculates that GvpC molecules span across multiple GvpA ribs to poetnically form "... straps of GvpC molecules, which bind the ribs together and thereby provide a sort of corset that prevents the gas vesicle from bulging out" - which from an engineering perspective sounds much like a ring stiffener. Additionally, Jost and Pfeifer [58] notes that GvpA/GvpC interaction is not detectable in split-GFP and pulldown assays, further suggesting that GvpC does not solely rely upon chemical bonding interactions to stabilize the GvpA ribs. We therefore speculate that ring stiffeners may act as an initial, zero-th order approximation for what GvpC may be doing to stiffen the gas vesicle- both to provide a lower bound on their stiffening effect by assuming purely mechanical interactions and to drive further research attention toward this area.

In this vein, the the number and distribution of stiffeners were optimized numerically to provide maximum stiffening- this allows us to avoid making a non-data driven choice for the number and distribution given the absence of experimental data.

4.6 Mechanism of Condensate-Driven GV Weakening

To obtain insight on the equilibrium properties of the GV wall, we evaluate the hydrogen bond content of the LML and LMV cases, see Figure 6A-D. In each of these plots, the number of hydrogen bonds in the LMV and LML cases are compared for different portions of GvpA, while schematics illustrate the location of the bonds. We find that across the board, the mean number of hydrogen bonds are smaller for the LML case, indicating less mechanical integrity. We also examine the secondary structure content in the LMV and LML cases for both the entire GvpA (see Figure 6E) and for the β-sheet region as defined by the PSIPRED prediction software (see Figure 6F) [59]. These plots confirm that a majority of residues in the designated β-sheet region participate in β-sheet structures, and indicate that the GV wall model remains intact even after extensive equilibration time. Although the presence of liquid water on the interior GvpA wall systematically decreases its structural stability, especially in primary features, the presence of water alone is unlikely to cause complete rupture. We hypothesize that wall weakening must be accompanied by buckling type instabilities to induce the final failure of a GV.

5 Conclusion

Overall, this work proposes two interlinked mechanisms that determines the final fate of gas vesicles in their role as biomolecular sensors and ultrasound reporters. We developed a model of the GvpA rib which is informed by experimental data, and has a more realistic structure than previous models. We have shown that a geometrically informed, elastic buckling model of GVs produces threshold pressures that fall near the critical collapse pressures observed in experiment.

We have also used heterogeneous nucleation theory and MD calculated wettability to show that condensation within the vesicle can lead to wall weakening at around the same pressure range for buckling. This suggests that condensation within the vesicle can either facilitate wall rupture under elastic buckling modes, or

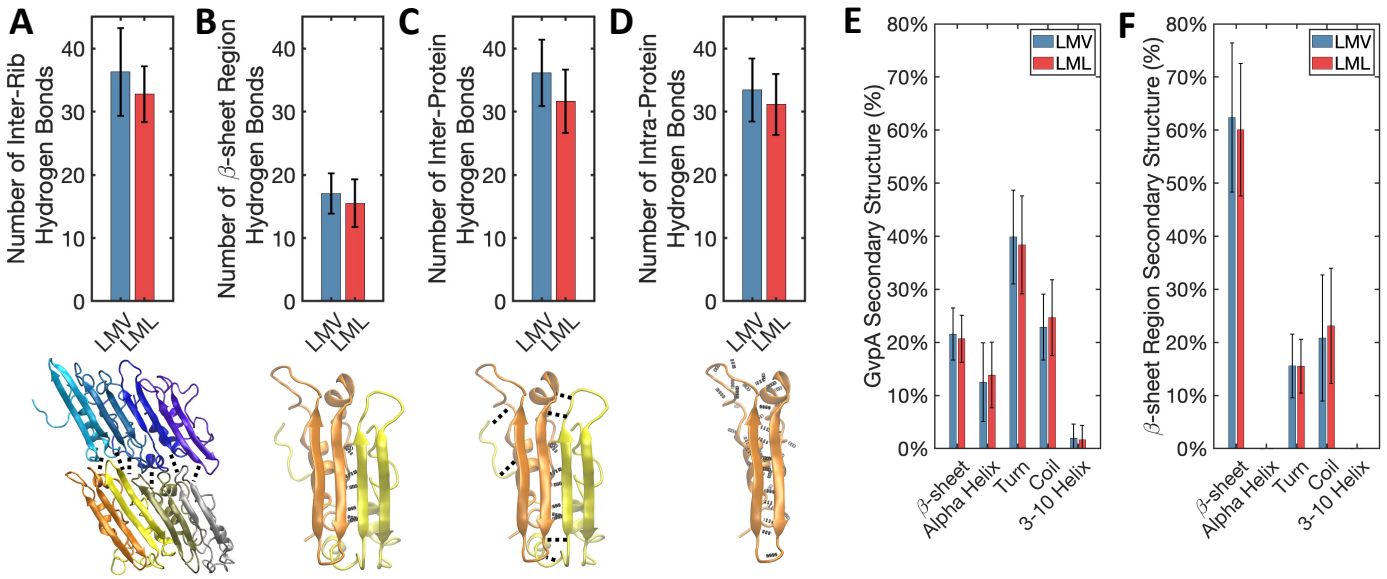

Fig. 6 Counting the number of A) inter-rib hydrogen bonds (in the axial direction) B) predicted β-sheet region only C) inter-protein hydrogen bonds, between GvpA in the same rib and D) intra-protein hydrogen bonds. Below, a schematic indicating the location of representative hydrogen bonds is included. E) The secondary structure of the entire GvpA and the F) predetermined β-sheet region is classified.

lead to an independent loss of echogenicity due to liquid filling of the interior.

Together, the two mechanisms may explain the observed dependence of GV collapse pressures on vesicle diameter. It also informs the design of GV structures that promote and extend the desired nonlinear response in imaging applications, where such a nonlinear regime is often truncated by vesicle collapse. Lastly, this hypothesis can account for the reversible variation of vesicle collapse pressure in the presence or absence of GvpC- that is, the original, higher collapse pressure can be recovered by binding GvpC to a previously stripped GV.

There are limitations to a computational model. For instance, inter-rib geometry has only been predicted using relatively crude MD models to date and the structure and organization of GvpC on the vesicle wall is completely unknown, although there have been some guesses[55]. Nevertheless, the performance these models suggest that further work with the GV structure at an all-atomistic level may be useful.

6 Conflicts of interest

There are no conflicts of interest to declare.

7 Acknowledgements

Sinan Keten and Martha Dunbar acknowledge funding from the Office of Naval Research (Grant no. N00014163175).

Notes and references

1 Walsby AE. Gas vesicles. Microbiological reviews. 1994 Sep;58(94).

2 Pfeifer F. Distribution, formation and regulation of gas vesicles. Nature Reviews Microbiology. 2012:705-15.

3 Offner S, Ziese U, Wanner G, Typke D, Pfeifer F. Structural characteristics of halobacterial gas vesicles. Microbiology. 1998:1331-42.

4 Walsby AE. The permeability of blue-green algal gas-vacuole membranes to gas. Proceedings of the Royal Society of London Series B Biological Sciences. 1969:235-55.

5 Englert C, Pfeifer F. Analysis of gas vesicle gene expression in Haloferax mediterranei reveals that GvpA and GvpC are both gas vesicle structural proteins. Journal of Biological Chemistry. 1993:9329-36.

6 Hayes P, Buchholz B, Walsby A. Gas vesicles are strengthened by the outer-surface protein, GvpC. Archives of Microbiology. 1992:229-34.

7 Shapiro MG, Goodwill PW, Neogy A, Yin M, Foster FS, Schaffer DV, et al. Biogenic gas nanostructures as ultrasonic molecular reporters. Nature Nanotechnology. 2014:311-6.

8 Cherin E, Melis JM, Bourdeau RW, Yin M, Kochmann DM, Foster FS, et al. Acoustic Behavior of Halobacterium salinarum Gas Vesicles in the High-Frequency Range: Experiments and Modeling. Ultrasound in Medicine and Biology. 2017:1016-30.

9 Lakshmanan A, Farhadi A, Nety SP, Lee-Gosselin A, Bourdeau RW, Maresca D, et al. Molecular Engineering of Acoustic Protein Nanostructures. ACS Nano. 2016:7314-22.

10 Bourdeau RW, Lee-Gosselin A, Lakshmanan A, Farhadi A, Kumar SR, Nety SP, et al. Acoustic reporter genes for noninvasive imaging of microorganisms in mammalian hosts. Nature. 2018:86-90.

11 Versluis M, Stride E, Lajoinie G, Dollet B, Segers T. Ultrasound Contrast Agent Modeling: A Review. Ultrasound in Medicine & Biology. 2020.

12 Song L, Wang G, Hou X, Kala S, Qiu Z, Wong KF, et al. Biogenic nanobubbles for effective oxygen delivery and enhanced

photodynamic therapy of cancer. Acta Biomaterialia. 2020.
13 Dassarma S, Dassarma P. Gas Vesicle Nanoparticles for Antigen Display. 2015:686-702.
14 Dunton PG, Mawby WJ, Shaw VA, Walsby AE. Analysis of tryptic digests indicates regions of GvpC that bind to gas vesicles of Anabaena flos-aquae. Microbiology. 2006:1661-9.
15 Kinsman R, Walsby AE, Hayes PK. GvpCs with reduced numbers of repeating sequence elements bind to and strengthen cyanobacterial gas vesicles. Molecular Microbiology. 1995:147-54.
16 Maresca D, Lakshmanan A, Lee-Gosselin A, Melis JM, Ni YL, Bourdeau RW, et al. Nonlinear ultrasound imaging of nanoscale acoustic biomolecules. Applied Physics Letters. 2017.
17 Talanquer V. Nucleation in Gas – Liquid Transitions. Journal of Chemical Education. 2002.
18 Batdorf SB. A Simplified Method of Elastic-Stability Analysis for Thin Cylindrical Shells. report. 1947.
19 Weingarten VI. Buckling of Thin-Walled Circular Cylinders. Special Publication. 1968.
20 Guzmán DL, Randall A, Baldi P, Guan Z. Computational and single-molecule force studies of a macro domain protein reveal a key molecular determinant for mechanical stability. Proceedings of the National Academy of Sciences. 2010.
21 Zhang S, Huang A, Bar-Zion A, Wang J, Mena OV, Shapiro MG, et al. The Vibration Behavior of Sub-Micrometer Gas Vesicles in Response to Acoustic Excitation Determined via Laser Doppler Vibrometry. Adv Funct Mater. 2020.
22 Ambartsumyan SA. Theory of Anisotropic Shells. 1961 Sep:1-396.
23 Patankar NA. Supernucleating surfaces for nucleate boiling and dropwise condensation heat transfer. Soft Matter. 2010:1613-20.
24 Jones PR, Elliott AR, Patankar NA. Sustaining Superheated Liquid within Hydrophilic Surface Texture. Langmuir. 2016:12947-53.
25 Zhao TY, Jones PR, Patankar NA. Thermodynamics of sustaining liquid water within rough icephobic surfaces to achieve ultra-low ice adhesion. Scientific Reports. 2019:1-12.
26 Strunk T, Hamacher K, Hoffgaard F, Engelhardt H, Zillig MD, Faist K, et al. Structural model of the gas vesicle protein GvpA and analysis of GvpA mutants in vivo. Molecular Microbiology. 2011:56-68.
27 Ezzeldin HM, Klauda JB, Solares SD. Modeling of the major gas vesicle protein , GvpA : From protein sequence to vesicle wall structure. Journal of Structural Biology. 2012:18-28.
28 Bayro MJ, Daviso E, Belenky M, Griffin RG, Herzfeld J. An amyloid organelle solid-state NMR evidence for cross-β assembly of gas vesicles. Journal of Biological Chemistry. 2012:3479-84.
29 Sivertsen AC, Bayro MJ, Belenky M, Griffin RG, Herzfeld J. Solid-state NMR evidence for inequivalent GvpA subunits in gas vesicles. Journal of molecular biology. 2009:1032-9.
30 Simons KT, Kooperberg C, Huang E, Baker D. Assembly of protein tertiary structures from fragments with similar local sequences using simulated annealing and bayesian scoring functions. Journal of Molecular Biology. 1997:209-25.
31 Humphrey W, Dalke A, Schulten K. vmd - Visual Molecular Dynamics. Journal of Molecular Graphics. 1996:33-8.
32 Brooks BRea. CHARMM: the biomolecular simulation program. Journal of computational chemistry. 2009:1545-614.
33 Huang MJA J. CHARMM36 all-atom additive protein force field: Validation based on comparison to NMR data. Journal of Computational Chemistry. 2013:2135-45.
34 Phillips JC, Braun R, Wang W, Gumbart J, Tajkhorshid E, Villa E, et al. Scalable molecular dynamics with NAMD. Journal of computational chemistry. 2005:1781-802.
35 Price DJ, Brooks CL. A modified TIP3P water potential for simulation with Ewald summation. The Journal of Chemical Physics. 2004:10096-103.
36 Frishman D, Argos P. Knowledge-based protein secondary structure assignment. Proteins: Structure, Function, and Bioinformatics. 1995:566-79.
37 Plimpton S. Fast Parallel Algorithms for Short-Range Molecular Dynamics. Journal of Computational Physics. 1995:1-19.
38 Molinero V, Moore EB. Water modeled as an intermediate element between carbon and silicon. Journal of Physical Chemistry B. 2009:4008-16.
39 Gautieri A, Buehler MJ, Redaelli A. Deformation rate controls elasticity and unfolding pathway of single tropocollagen molecules. Journal of the Mechanical Behavior of Biomedical Materials. 2009:130-7.
40 Marmottant P, van der Meer S, Emmer M, Versluis M, de Jong N, Hilgenfeldt S, et al. A model for large amplitude oscillations of coated bubbles accounting for buckling and rupture. The Journal of the Acoustical Society of America. 2005 2023/01/03;118(6):3499-505. Available from: https://doi.org/10.1121/1.2109427.
41 Keten S, Buehler MJ. Nanostructure and molecular mechanics of spider dragline silk protein assemblies. Journal of The Royal Society Interface. 2010:1709-21.
42 Walsby AE, Bleything A. The Dimensions of Cyanobacterial Gas Vesicles in Relation to Their Efficiency in Providing Buoyancy and Withstanding Pressure. Microbiology. 1988:2635-45.
43 Dutka P, Malounda D, Metskas LA, Chen S, Hurt RC, Lu GJ, et al. Measuring gas vesicle dimensions by electron microscopy. The Protein Society. 2021:1-6.
44 Hayes PK, Lazarus CM, Bees A, Walker JE, Walsby AE. The protein encoded by gvpC is a minor component of gas vesicles isolated from the cyanobacteria Anabaena flos-aquae and Microcyctis sp. Molecular Microbiology. 1988:545-52.
45 Dunton PG, Walsby AE. The diameter and critical collapse pressure of gas vesicles in Microcystis are correlated with GvpCs of different length. FEMS Microbiology Letters. 2005:37-43.
46 Bright DI, Walsby AE. The relationship between critical pressure and width of gas vesicles in isolates of Planktothrix

rubescens from Lake Zurich. Microbiology. 1999.
47 Beard SJ, Handley BA, Walsby AE. The relationship between critical pressure and width of gas vesicles in isolates of Planktothrix rubescens from Lake Zurich. FEMS Microbiol Lett. 2002.
48 Hayes PK, Walsby AE. The inverse correlation between width and strength of gas vesicles in cyanobacteria. British Phycological Journal. 1986:191-7.
49 Lemmon E, McLinden M, Friend D. NIST Chemistry WebBook, NIST Standard Reference Database Number 69. National Institute of Standards and Technology; 2012. .
50 Kuznetsova LA, Coakley WT. Applications of ultrasound streaming and radiation force in biosensors. Biosensors and Bioelectronics. 2007:1567-77.
51 Yosiok K, Kawasima Y. Acoustic radiation pressure on a compressible sphere. Acustica. 1955:167-73.
52 Hasegawa T, Hino Y, Annou A, Noda H, Kato M, Inoue N. Acoustic radiation pressure acting on spherical and cylindrical shells. The Journal of the Acoustical Society of America. 1993:154-61.
53 Rooney JA. Shear as a mechanism for sonically induced biological effects. J Acoust Soc Am. 1972:1718-24.
54 Sharma GS, Marsick A, Maxit L, Skvortsov A, MacGillivray I, Kessissoglou N. Acoustic radiation from a cylindrical shell with a voided soft elastic coating. The Journal of the Acoustical Society of America. 2021:4308-14.
55 Buchholz BE, Hayes PK, Walsby AE. The distribution of the outer gas vesicle protein, GvpC, on the Anabaena gas vesicle, and its ratio to GvpA. Journal of General Microbiology. 1993:2353-63.
56 Offner S, Wanner G, Pfeifer F. Functional studies of the gvpACNO operon of Halobacterium salinarium reveal that the GvpC protein shapes gas vesicles. Journal of Bacteriology. 1996:2071-8.
57 Walsby AE, Revsbech N, Griffel DH. The gas permeability coefficient of the cyanobacterial gas vesicle wall. Microbiology-sgm. 1992:837-45.
58 Jost A, Pfeifer F. Interaction of the gas vesicle proteins GvpA, GvpC, GvpN, and GvpO of Halobacterium salinarum. Front Microbiol. 2022.
59 McGuffin LJ, Bryson K, Jones DT. The PSIPRED protein structure prediction server. Bioinformatics. 2000:404-5.